SOLAR PANELS AREA ESTIMATION USING THE SPACEBORNE IMAGING SPECTROMETER DESIS: OUTPERFORMING MULTISPECTRAL SENSORS

D. Cerra[a, *], C. Ji[b,c], U. Heiden[a]

[a] DLR, German Aerospace Center, Remote Sensing Technology Institute - (daniele.cerra, uta.heiden)@dlr.de
[b] DLR, German Aerospace Center, DFD Institute
[c] University of Leipzig, Remote Sensing Center for Earth System Research - chaonan.ji@uni-leipzig.de

Commission I, WG I/1

KEY WORDS: DESIS, Hyperspectral, Area estimation, Spectral Unmixing, Imaging Spectrometry, Photovoltaic panels.

ABSTRACT:

Solar photovoltaic power plants are in rapid expansion throughout the world, with the total area occupied by panels being linked to the total electrical power produced. This paper considers this case as an instance of the generic problem of estimating the total area occupied by a class of interest in spaceborne hyperspectral images. As the spatial resolution characterizing these sensors is too coarse, spectral unmixing techniques identify the contribution of a specific material to the spectrum related to a single image element. Final results are obtained by summing all contributions in an area of interest, and favourably compared to pixel-based detection, also using higher resolution Sentinel-2 data. The data used in this paper are acquired by the currently operative DESIS sensor, mounted on the International Space Station, encouraging the use of spaceborne imaging spectrometers for such applications.

1. INTRODUCTION

An imaging spectrometer, also known as hyperspectral sensor, quantifies the backscattered solar radiation from a resolution cell on ground across narrow and often contiguous bands. The resulting images usually offer a higher spectral and lower spatial resolution with respect to more traditional multispectral sensors, usually characterized by fewer, broader bands. Until recently, state-of-the-art imaging spectrometers have mostly been airborne, with a number of experimental successful spaceborne missions being launched in the past 20 years, the most relevant probably being the Hyperion sensor on board of the Earth Observing-1 (EO-1) satellite (Khurshid et al., 2006). Recent years are witnessing the launch of several new spaceborne sensors, such as the DLR Earth Sensor Imaging Spectrometer (DESIS) (Alonso et al., 2019), mounted on board of the International Space Station (ISS), with new missions being currently under development, such as EnMAP (Guanter et al., 2015).

Since the early years of hyperspectral imaging exploitation, attention has been given to the added capabilities of this family of sensors with respect to multispectral ones. On the one hand, hyperspectral data excel at identifying materials based on their fine spectral capabilities, and at retrieving important physical parameters observable mainly in narrow bands. This led researchers to obtain results superior to the ones based on multispectral data, in several areas of study such as the analysis of vegetation (Lee et al., 2004), (Asner et al., 2008), (Mariotto et al., 2013), water (Phinn et al., 2008), soil (Stevens et al., 2012), wetlands (Adam et al., 2010), and forests (Awad, 2018). On the other hand, classical applications heavily driven by statistical analysis such as supervised classification have witnessed limited increase in the accuracy of the results (Xu and Gong, 2007). Among several factors, this is due to the strong correlation of spectral bands in broad spectral ranges, causing the real dimensionality of the information contained in the data (also known as virtual dimensionality (Drumetz et al., 2016)) to be much lower than the total number of bands available; furthermore, the limited signal-to-noise Ratio (SNR) inherent to narrow bands analysis pose additional hindrances; additionally, the large volumes of data introduce the so-called curse of dimensionality, which requires large amounts of training data to be collected for accurate results, and are also difficult to pre-process and explore.

In this paper, we report our first results on a different family of applications in which spaceborne imaging spectrometers may outperform multispectral sensors: the estimation of surfaces covered by a target of interest mostly present in mixed pixels. A mixed pixel is defined as an image element in which a target or any number of classes of interest covers only a fraction of the resolution cell. In this case, multiplying the area in meters of a single pixel by the number of pixels detected by any algorithm, even if detection is very accurate, leads to an overestimation of the area. Hyperspectral image processing offers efficient methods to tackle this problem, such as spectral unmixing, which at the same time recognizes the materials present within a single pixel, represented by their pure spectra usually known as endmembers, and also the amount of that pixel covered by each material, known as fractional abundance (Bioucas-Dias et al., 2012). In order to perform spectral unmixing successfully and accurately, the number of available spectral bands in the data must ideally be much larger than the number of materials present in the scene, making this technique difficult to apply using multispectral sensors.

We report in this paper the first results of applying surface area estimation results based on spectral unmixing with DESIS data on the solar Photovoltaic (PV) power plant of Oldenburg, Germany, for which ground truth is available and sub-meter resolution would be needed in order to estimate the surface with traditional detection or classification approaches. We report not only the accurate results obtained with DESIS, but also how traditional multispectral sensors such as Sentinel-2 fail for this task. The paper is structured as follows. Section 2. introduces the site of interest and the available data, while Section 3. presents our proposed surface area estimation based on spectral unmixng, and Section 4. compares results obtained with hyper- and multi-spectral sensors using both pixel-based and unmixing methods. We conclude in Section 5..

*Corresponding author.

2. DATASETS

Our study is carried out on a large PV power plant located on the old airfield in Oldenburg in the northwest of Germany. Imaging spectrometer data at both high resolution (HySpex, airborne) and low resolution (DESIS, spaceborne) have been used and are described in this section, along with Sentinel-2 multispectral spaceborne data and ground truth in vectorial format for validation.

2.1 HySpex

High resolution imaging spectrometer data are provided by a flight campaign carried out in July 2018 covering Oldenburg with the HySpex system, composed by two cameras covering the spectral ranges of visible near infrared (VNIR) and short-wave infrared (SWIR) region. The VNIR sensor has a spectral range from 416 to 992 nm with 160 channels at a Ground Sampling Distance (GSD) of 0.6 m, while the SWIR has 256 channels in the 1000-2500 nm range, with a GSD of 1.2 m. The VNIR and SWIR images were co-registered (Schwind et al., 2014) and resampled to a GSD of 1.2 m. Data have been converted to surface reflectance using the ATCOR4 atmospheric correction software (Richter et al., 2010) as described in (Köhler, 2016). A true color composite for a subset of the HySpex dataset is reported in Fig. 1, with overlaid areas containing PV panels in vectorial format.

2.2 DESIS

The DESIS spectrometer acquires 235 bands in the spectral range 400-1000 nm, with a fine spectral resolution of 2.35 nm, and a GSD of 30 m (Alonso et al., 2019). As DESIS is mounted on the ISS, it has a nearly circular orbit with an average altitude of 400 kilometres, with extremely high latitudes excluded from its acquisition capabilities.

The DESIS sensor has been tasked to acquire data on the Oldenburg power plant, and an image with clear conditions was successfully archived on the 9th of October 2021. In spite of the temporal gap with the HySpex and Sentinel-2 data, the targets of interest have not undergone major changes and the image can be employed for a results comparison. The image has been atmospherically corrected using the Python-based Atmospheric Correction (PACO) software (de los Reyes et al., 2020, Alonso et al., 2019). A true color RGB composition is reported for the subset of interest in Fig. 2.

2.3 Sentinel-2

We employed a clear image in surface reflectance (Level 2A) acquired by the Sentinel-2A sensor on the 27th of July 2018. As Sentinel-2 features spectral bands at different GSD, two different stacks were created to be later analysed by different algorithms:

1. A stack containing a total of 8 spectral bands: the 4 originally at 10 m GSD (2, 3, 4, and 8), plus the bands at 20 m which overlap DESIS spectral range (bands 5, 6, 7, and 8A). The stack has been resampled to 20 m GSD. Therefore, bands 11 and 12 which fall outside of DESIS spectral range have not been considered, along with bands at 60 m GSD. This was done in order to focus the comparison on the tradeoff between spatial and spectral resolution keeping the spectral range unaltered.

2. In order to exploit the higher spatial resolution of bands at 10 m GSD, a second stack was used containing only bands 2, 3, 4, and 8.

2.4 Validation data

The ground truth initially comes from official register data. As some panels annotations were including areas of future expansion, these have been manually removed beforehand using the high resolution HySpex image as reference, without altering the size and shape of the remaining panels. An overlay of the reference data on a HySpex true color composite subset is reported in Fig. 1. The figure shows how panels in the west side of the solar garden present larger gaps among them with respect to the panels to the east, which are deployed in a denser arrangement. This aspect is important as we expect a change in the pixel percentage occupied by the panels in low resolution data.

3. SURFACE ESTIMATION VIA SPECTRAL UNMIXING

The process of spectral unmixing (SU) decomposes the spectrum associated to a pixel in signals typically belonging to macroscopically pure materials, or endmembers. The contribution of a given material to the spectrum of an image element is a fractional quantity, usually named abundance. The unmixing process provides accurate information at sub-pixel level on a hyperspectral scene, and is widely used in several application ranging from classification and target detection to denoising and image fusion (Bioucas-Dias et al., 2012, Cerra et al., 2014, Roessner et al., 2001). Usually, the full process of spectral unmixing includes the estimation of the number of materials present in the scene, the selection of their related spectra (endmember extraction), and the estimation of the fractional coverage of each pixel in terms of the pure materials present in a resolution cell (abundance estimation).

Linear spectral unmixing (LSU) is the most widely adopted model for these methods, and assumes that the contribution of an endmember to a given pixel's spectrum is proportional to the relative fractional abundance. LSU models the spectrum of a pixel $\mathbf{p}$ with m bands as a linear combination of n reference spectra $\mathbf{S} = [s_1, s_2, \ldots, s_n]$, weighted by their n scalar fractional abundances $\mathbf{x} = [x_1, x_2, \ldots, x_n]^T$, plus a residual vector $\mathbf{r}$ containing noise and the portion of the signal which cannot be represented in terms of the basis vectors of choice:

$$\mathbf{p} = \sum_{i=1}^{n} x_i s_i + r = \mathbf{S}\mathbf{x} + \mathbf{r} \tag{1}$$

LSU has been applied for target detection in (Manolakis et al., 2001), and we apply it to the problem of area estimation as follows. Given a spectral library $\mathbf{S}$ containing the material of interest k with associated spectrum s_k, the total area A_k occupied by k in an image with a total number of pixels $numel$ is estimated as the sum of the abundances of s_k in each pixel:

$$A_k = \sum_{i=1}^{numel} x_k \tag{2}$$

In order to mitigate the impact of noise and avoid considering non-relevant entries, abundances $x_k < 0.15$ are set to 0. In order to derive abundance maps quantifying the fraction of each image element covered by the class of interest, it is needed to have a representative spectral library for the scene, containing all endmembers related to the materials present in the image. Automatic endmembers extraction methods exist and are widely used with varying degree of success, according to the scene type, data quality, spatial and spectral resolution, and scale of the materials of

Figure 1: Detail of ground truth in vectorial format for solar panels (red), overlaid on HySpex true color composite.

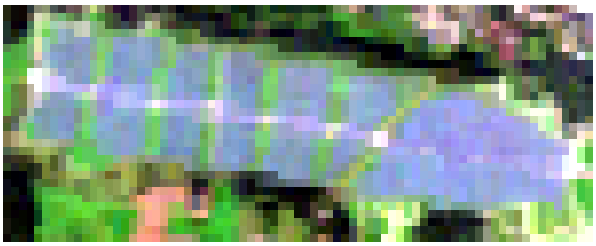

Figure 2: DESIS true color composite: bands 94 (640 nm), 59 (550 nm), 24 (470 nm).

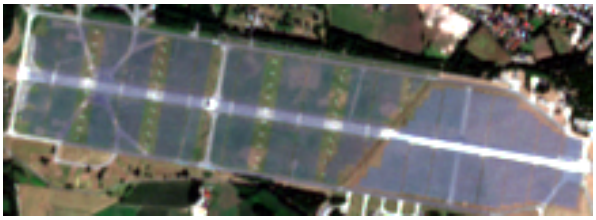

Figure 3: Sentinel-2 true color composite (bands 4, 3, 2).

interest (Bioucas-Dias et al., 2012). These methods usually need the number of materials in the scene, which can also be estimated using algorithms such as HySime (Drumetz et al., 2016).

In order to estimate the abundances, we apply Non-negative Least Squares (NNLS) to the input image and the described spectral library. The code is a modified faster version of the implementation contained in the Matlab Hyperspectral Toolbox (Isaac, 2022) and is available on demand. The LSU problem in eq. 2 becomes then its constrained version with $x_k \geq 0, \forall k$. NNLS exhibits the best performance among commonly used optimization methods for this problem (Cerra et al., 2021) and yields a solution which is naturally sparse in the abundance vector, limiting estimation errors introduced by noise or enforcing the sum-to-one constraint in presence of materials not present in the spectral library (Iordache et al., 2011).

The output is a fraction of each pixel which is covered by each material, and can be multiplied by the size in m^2 of an image element in order to estimate the total surface.

3.1 Pixel-based techniques

We consider algorithms with binary outputs operating pixelwise, in order to compare the spectral unmixing surface estimation to pixel-based approaches, selecting both a traditional and a recent approach, which was developed ad hoc for PV detection. For the following algorithms, the total area A_k for a material k is just computed as $A_k = A_p \times N_k$, where A_p is the area in meters of a single image element and N_k the number of pixels assigned to material k.

3.1.1 Maximum Likelihood Maximum Likelihood (ML) has been used for decades in supervised remote sensing classification (Strahler, 1980), mostly with multispectral data. In order to detect a specific class, ML assumes probability distributions of the pixel values of a specific class to have Gaussian distributions, and computes the probability that the values of a specific pixel have been generated by those distributions.

3.1.2 Spectral Features A recent approach was developed to detect PV specifically from high-resolution imaging spectrometer data, which was validated on a large database in (Ji et al., 2021). Due to spectral range limitations, only three of the six spectral indices were used in this study, namely average reflectance in the VNIR (aVNIR), PolyEthylene Peak (PEP), and PolyEthylene Peak in the visible range (VPEP). We refer to this method as "Spectral Features", as it relies on a combination of spectral indices designed to further separate PV modules from spectrally similar targets such as hydrocarbon roof materials.

4. RESULTS

After checking the validation data (ref. Section 2.) the total area occupied by solar panels in the area was derived based on the vectorial data attributes as 22.64 hectares (ha).

4.1 Pixel-based methods

The total area estimated as being covered by a specific class of interest for the different kinds of sensors and GSDs has been computed.

Firstly, results obtained based on Spectral Features (Ji et al., 2021) were used to estimate the total area related to detected PV pixels in the high resolution HySpex image in Fig. 1. The approximation of such tested pixel-based method at a GSD of 1.2 m results accurate, with an underestimation of the area of 0.8 ha only (see Table 1).

Subsequently, both the ML and the Spectral Features approach have been applied to DESIS and Sentinel-2 data (Table 1). For

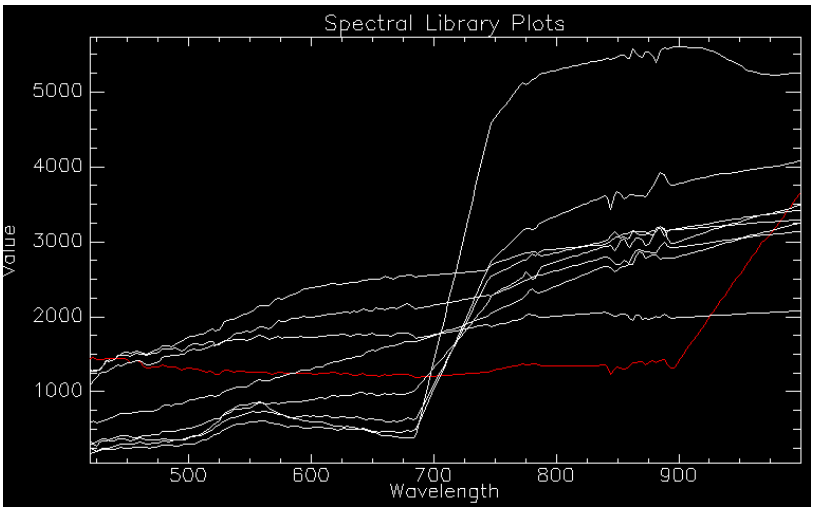

Figure 4: Spectral library from HySpex data resampled to DESIS spectral bands. The unit of measure is reflectance, multiplied by 10^4. The solar panels class of interest is reported in red. Spectra in white include 4 vegetation spectra, plus 2 spectra belonging to soil, and 2 to man-made structures.

the latter, the stack of 4 bands at 10 meters has been preferred in order to exploit the higher GSD of these bands for ML, while the stack at 20 m was required by the Spectral Features method. At 10 m GSD, results of Sentinel-2 classification using ML (Fig. 6) already present an overestimation above 100%. The overestimation increases further when switching to the 20 m GSD Sentinel-2 stack used by the Spectral Features method (Fig. 8), and goes above 170% when considering ML classification of DESIS data at 30 m GSD (Fig. 5). On the other hand, the overestimation introduced by Spectral Features decreases in DESIS, in spite of the worse spatial resolution (Fig. 7). This suggests that the spectral resolution could be more important for the related spectral indices, which lose performance when applied to broadband multispectral data.

4.2 Unmixing-based methods

As described in Section 3., a spectral library containing the spectra of all relevant materials present in a scene should be available, in order to estimate the total surface covered by a material of interest. Usually, such spectra are obtained directly from the image by selecting pure pixels acquired over homogeneous areas for each material, or automatically extracting them with endmember extraction algorithms. Nevertheless, the GSD of 30 m characterizing DESIS prevents any pure pixel containing only solar panels to be present in the scene. As results clear from Fig. 1, all panels are much smaller in size and between different rows other materials such as vegetation and soil can be observed, which would be included in the extracted endmembers, degrading the quality of the spectral library and in turn of the results. Therefore, we manually selected 9 relevant spectra from the HySpex image at 1.2 m GSD instead, and resampled their spectra to DESIS bands. Only one spectrum is selected for PV panels, while the other spectra include 2 grass, 2 forest, 2 soil, and 2 impervious surfaces. In order to match HySpex range to DESIS, only the visible near infrared (VNIR) sensor is considered, as the SWIR falls outside DESIS spectral range (Fig. 4). The library is also resampled to match Sentinel-2 broadband spectra, based on central frequencies and full width half maximum (FWHM) values of each band.

Results obtained on DESIS data reported in Fig. 9 are surprising, as the real size of the panels is retrieved with an error below 0.05%. It must be specified that this also happens because of compensation of false alarms outside of the panels area with underestimations on the panels. In order to take this into account, an additional result is reported (Spectral Unmixing - masked) in which the area outside of the solar garden was completely masked out. In this case, results are perfectly equal to the ones obtained with HySpex, which has a spatial resolution 25 times larger (meaning that we have 625 HySpex pixels for a single DESIS pixel), with an overall error of 3.66%. In the image, it can be seen how the abundance of PV panels gets higher in the eastern block of the solar garden, where the panels are more densely deployed. The average values for the abundances in the western and eastern parts of the image are 0.3 and 0.4, respectively. As previous experiments were considering a detected pixel as having abundance 1, we can justify the huge difference in final results. It must be remarked that it is not possible to compute an Intersection over Union (IoU) or a more accurate error estimate, as this is not allowed by DESIS coarse spatial resolution: in laymen's terms, it is not possible to locate the portion containing PV panels within a single DESIS resolution cell.

On the other hand, unmixing experiments using Sentinel-2 data yield a complete failure. In this setting, the same spectral library resampled to the spectral characteristics of the image is used, and results are reported in Fig. 10. Noise is evident in the results, and the main sealed road connecting the area horizontally is misdetected as PV panels. As the number of endmembers in the library (9) is larger than the number of Sentinel-2 bands employed (8), the inversion problem is mathematically unstable. Furthermore, the relevant spectral features may not be resolved in Sentinel-2 broadbands.

5. CONCLUSIONS

In this paper we assessed the potential of spaceborne imaging spectrometer such as DESIS to estimate the surface covered by a material of interest in a mixed pixel environment. The surface is estimated as the pixel-wise sum of all fractional abundances for the endmember linked to the target material. The abundances are derived by spectral unmixing methods, and yield estimates very close to the real size of the solar panels considered in our test area in Oldenburg, Germany.

The method requires a spectral library containing the material of interest and representative materials in the scene. This must be available beforehand, if no pure pixels are present in the scene. Usually, for background materials such as grass, trees, and soil, it

Figure 5: DESIS Maximum Likelihood results. Solar panels class is reported in red.

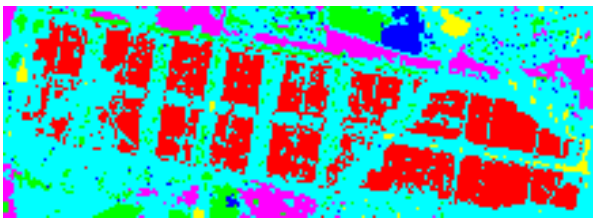

Figure 6: Sentinel-2 Maximum Likelihood results. Solar panels class is reported in red.

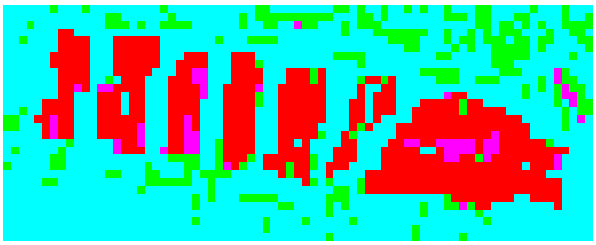

Figure 7: DESIS spectral features. Solar panels class is reported in red.

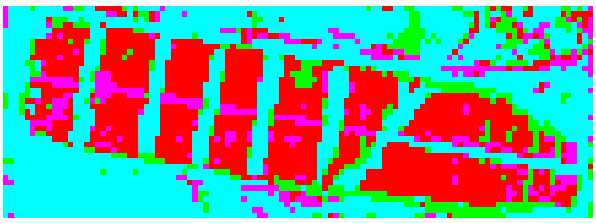

Figure 8: Sentinel-2 Spectral Features results. Solar panels class is reported in red.

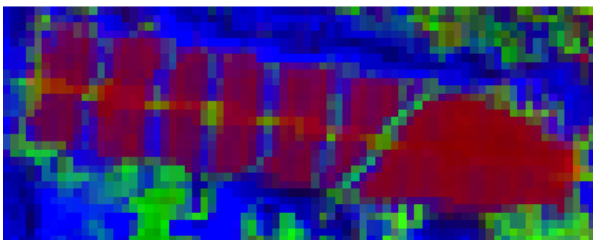

Figure 9: DESIS unmixing results. The PV abundance map is reported in red, while aggregates of other materials appear in blue and green.

Sensor	**GSD** (m)	**No. bands**	**Method**	**Area** (ha)	Error (%)
HySpex	1.2	158	SF	21.84	**-3.66**
Sentinel-2	10	4	ML	45.5	+101
Sentinel-2	20	8	SF	55.8	+146
			SU	15.06	-33.5
DESIS	30	235	ML	61.3	+171
			SF	49.14	+117
			SU	**22.63**	**-0.05**
			SU (masked)	**21.84**	**-3.66**
Ground Truth				**22.64**	

Table 1: Area estimation results for the Oldenburg photovoltaic panels dataset. Area estimation in hectares and relative error in percentage are reported according to sensor, Ground Sampling Distance (GSD), number of spectral bands, and optimal technique used for the kind of data at hand: Maximum Lilkelihood (ML), Spectral Features (SF), or Spectral Unmixing (SU). Spectral Unmixing (masked) indicates the area estimation after filtering out false alarms by not considering pixels outside of the solar garden. Sentinel-2 is used at two different resolutions for different techniques. The last row reports the target area.

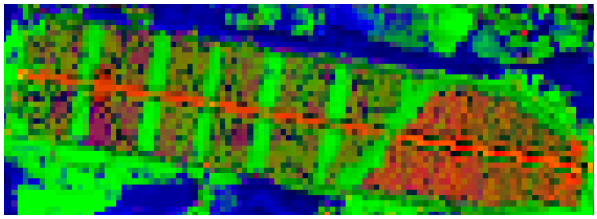

Figure 10: Sentinel-2 unmixing results. The PV abundance map is reported in red, while aggregates of other materials appear in blue and green.

is possible to identify such pure pixels in the scene also at coarse resolution. Therefore, the availability of a spectral library related to the specific kind of PV present in the scene could suffice.

As used abundance estimation algorithms do not "weight" the spectral bands, we cannot provide information on the spectral range which was prominent in identifying the contribution of the solar panels to each single resolution cell. About this aspect, an interested reader is remanded to (Ji et al., 2021), investigating the best narrow bands to classify PVs.

This is a contribution to the long and interesting quest for applications in which imaging spectrometers may outperform traditional broadband multispectral sensors. The aim of this work is to show how data with high spectral and low spatial resolution may outperform traditional broadband MS sensors for some specific task. In this sense, results appear very encouraging. On the one hand, specific sub-pixel analysis (unmixing-based techniques) completely fails when applied to multispectral sensors. On the other hand, sub-pixel analysis applied to DESIS data outperforms pixel-based classification or target detection algorithms carried out at higher spatial resolution, which yield in our experiments an overestimation of the area occupied by the targets of interest of at least 100%.

In the future, a spectral library of PV panels could be considered in order to carry out similar experiments on different areas and types of solar panels, yielding a more meaningful assessment of the results.

ACKNOWLEDGEMENTS

The pre-processing of the HySpex data was carried out by OpAIRS of the Remote Sensing Technology Institute (IMF) of German Aerospace Center (DLR). The original ground truth data are from official register data © GeoBasis-DE / BKG (2021), with associated terms of use available at
http://sg.geodatenzentrum.de/web_public/nutzungsbedingungen.pdf.

REFERENCES

Adam, E., Mutanga, O. and Rugege, D., 2010. Multispectral and hyperspectral remote sensing for identification and mapping of wetland vegetation: a review. Wetlands Ecology and Management 18(3), pp. 281–296.

Alonso, K., Bachmann, M., Burch, K., Carmona, E., Cerra, D., de los Reyes, R., Dietrich, D., Heiden, U., Hölderlin, A., Ickes, J., Knodt, U., Krutz, D., Lester, H., Müller, R., Pagnutti, M., Reinartz, P., Richter, R., Ryan, R., Sebastian, I. and Tegler, M., 2019. Data products, quality and validation of the dlr earth sensing imaging spectrometer (desis). Sensors.

Asner, G. P., Knapp, D. E., Kennedy-Bowdoin, T., Jones, M. O., Martin, R. E., Boardman, J. and Hughes, R. F., 2008. Invasive species detection in hawaiian rainforests using airborne imaging spectroscopy and lidar. Remote Sensing of Environment 112(5), pp. 1942–1955. Earth Observations for Terrestrial Biodiversity and Ecosystems Special Issue.

Awad, M., 2018. Forest mapping: a comparison between hyperspectral and multispectral images and technologies. Journal of Forestry Research 29, pp. 1395–1405.

Bioucas-Dias, J. M., Plaza, A., Dobigeon, N., Parente, M., Du, Q., Gader, P. and Chanussot, J., 2012. Hyperspectral unmixing overview: Geometrical, statistical, and sparse regression-based approaches. IEEE Journal of Selected Topics in Applied Earth Observations and Remote Sensing 5(2), pp. 354–379.

Cerra, D., Müller, R. and Reinartz, P., 2014. Noise reduction in hyperspectral images through spectral unmixing. IEEE Geoscience and Remote Sensing Letters 11(1), pp. 109–113.

Cerra, D., Pato, M., Alonso, K., Köhler, C., Schneider, M., de los Reyes, R., Carmona, E., Richter, R., Kurz, F., Reinartz, P. and et al., 2021. Dlr hysu—a benchmark dataset for spectral unmixing. Remote Sensing 13(13), pp. 2559.

de los Reyes, R., Langheinrich, M., Schwind, P., Richter, R., Pflug, B., Bachmann, M., Müller, R., Carmona, E., Zekoll, V. and Reinartz, P., 2020. Paco: Python-based atmospheric correction. Sensors.

Drumetz, L., Veganzones, M. A., Marrero Gómez, R., Tochon, G., Mura, M. D., Licciardi, G. A., Jutten, C. and Chanussot, J., 2016. Hyperspectral local intrinsic dimensionality. IEEE Transactions on Geoscience and Remote Sensing 54(7), pp. 4063–4078.

Guanter, L., Kaufmann, H., Segl, K., Foerster, S., Rogass, C., Chabrillat, S., Kuester, T., Hollstein, A., Rossner, G., Chlebek, C. et al., 2015. The enmap spaceborne imaging spectroscopy mission for earth observation. Remote Sensing 7(7), pp. 8830–8857.

Iordache, M.-D., Bioucas-Dias, J. and Plaza, A., 2011. Sparse unmixing of hyperspectral data. IEEE Transactions on Geoscience and Remote Sensing 49, pp. 2014–2039.

Isaac, 2022. Matlab hyperspectral toolbox.

Ji, C., Bachmann, M., Esch, T., Feilhauer, H., Heiden, U., Heldens, W., Hueni, A., Lakes, T., Metz-Marconcini, A., Schroedter-Homscheidt, M., Weyand, S. and Zeidler, J., 2021. Solar photovoltaic module detection using laboratory and airborne imaging spectroscopy data. Remote Sensing of Environment 266, pp. 112692.

Khurshid, S., Staenz, K., Sun, L., Neville, R., White, H., Abdou, B., Champagne, C. and Hitchcock, R., 2006. Processing of eo-1 hyperion data. Canadian Journal of Remote Sensing 32, pp. 84–97.

Köhler, C. H., 2016. Airborne imaging spectrometer hyspex. Journal of large-scale research facilities JLSRF 2(A93), pp. 1–6.

Lee, K.-S., Cohen, W. B., Kennedy, R. E., Maiersperger, T. K. and Gower, S. T., 2004. Hyperspectral versus multispectral data for estimating leaf area index in four different biomes. Remote Sensing of Environment 91(3-4), pp. 508–520.

Manolakis, D., Siracusa, C. and Shaw, G., 2001. Hyperspectral subpixel target detection using the linear mixing model. IEEE transactions on geoscience and remote sensing 39(7), pp. 1392–1409.

Mariotto, I., Thenkabail, P. S., Huete, A., Slonecker, E. T. and Platonov, A., 2013. Hyperspectral versus multispectral crop-productivity modeling and type discrimination for the hyspiri mission. Remote Sensing of Environment 139, pp. 291–305.

Phinn, S., Roelfsema, C., Dekker, A., Brando, V. and Anstee, J., 2008. Mapping seagrass species, cover and biomass in shallow waters: An assessment of satellite multi-spectral and airborne hyper-spectral imaging systems in moreton bay (australia). Remote sensing of Environment 112(8), pp. 3413–3425.

Richter, R., Schläpfer, D. and Müller, A., 2010. Operational atmospheric correction for imaging spectrometers accounting for the smile effect. IEEE Transactions on Geoscience and Remote sensing 49(5), pp. 1772–1780.

Roessner, S., Segl, K., Heiden, U. and Kaufmann, H., 2001. Automated differentiation of urban surface based on airborne hyperspectral imagery. Geoscience and Remote Sensing, IEEE Transactions on 39, pp. 1525 – 1532.

Stevens, A., Miralles, I. and van Wesemael, B., 2012. Soil organic carbon predictions by airborne imaging spectroscopy: Comparing cross-validation and validation. Soil Science Society of America Journal 76(6), pp. 2174–2183.

Strahler, A. H., 1980. The use of prior probabilities in maximum likelihood classification of remotely sensed data. Remote sensing of Environment 10(2), pp. 135–163.

Xu, B. and Gong, P., 2007. Land-use/land-cover classification with multispectral and hyperspectral eo-1 data. Photogrammetric Engineering & Remote Sensing 73(8), pp. 955–965.